

Article

Analysis of the Phenomena Causing Weave and Wobble in Two-Wheelers

Francesco Passigato ^{1,*}, Andreas Eisele ¹, Dirk Wisselmann ², Achim Gordner ²
and Frank Diermeyer ¹

¹ Chair of Automotive Technology, Technical University of Munich, 85748 Garching bei München, Germany; andreas.eisele@tum.de (A.E.); diermeyer@ftm.mw.tum.de (F.D.)

² BMW Group, 80937 Munich, Germany; dwisselmann@t-online.de (D.W.); Achim.Gordner@bmw.de (A.G.)

* Correspondence: francesco.passigato@tum.de

Received: 24 August 2020; Accepted: 24 September 2020; Published: 29 September 2020



Abstract: The present work follows in the tracks of previous studies investigating the stability of motorcycles. Two principal oscillation modes of motorcycles are the well-known wobble and weave modes. The research in this field started about fifty years ago and showed how different motorcycle parameters influence the stability of the mentioned modes. However, there is sometimes a minor lack in the physical analysis of why a certain parameter influences the stability. The derived knowledge can be complemented by some mechanical momentum correlations. This work aims to ascertain, in depth, the physical phenomena that stand behind the influence of fork bending compliance on the wobble mode and behind the velocity dependence of the weave damping behaviour. After a summary of the relevant work in this field, this paper presents different rigid body simulation models with increasing complexity and discusses the related eigenvalue analysis and time behaviour. With these models, the mentioned modes are explained and the physical phenomena only partly covered by the literature are shown. Finally, the influence of the rider model on weave and wobble is presented.

Keywords: two-wheeler; vehicle dynamic modelling; wobble; weave; fork bending compliance; rider influence

1. Introduction

Motorcycle dynamics have always been an extensive research topic due to the complexity and the influence on the riders' safety. The knowledge used to develop a stable motorcycle chassis comes, to a certain extent, from experience or sensitivity analysis which sometimes lack physical and theoretical understanding of the hidden phenomena. This paper wants to clarify these phenomena, in particular with regard the understanding of the effect of the front fork bending compliance and of the weave damping behaviour with changing speed.

Two of the principal eigenmodes of a motorcycle are known as wobble and weave. The first one includes almost solely the rotation of the front assembly about the steering axis whose frequency is in the range between 7 and 10 Hz depending on the motorcycle's parameters [1]; the second one is more complex, and when affected by this mode, the motorcycle shows roll, yaw, steering-head rotation and lateral displacement [2].

The starting point for this work is an observation resulting from the comparison of experience in reality and simulation results. Using the eigenvalue analysis, the earlier motorcycle models, such as the model of Sharp [3] which only includes a tyre model but no compliances, show a stable wobble mode in the lower speed range (up to 80 km h⁻¹), and this mode becomes unstable in the higher speed range. However, the experience with a real motorcycle shows an almost opposite behaviour: lower stability (or even instability) at low speed and increasing stability at higher speed. This was demonstrated

through measurements on a real motorcycle by Koch [4]. Previous research addressed this apparent incompatibility between simulation and reality, concluding that the front fork bending compliance is a key parameter when studying wobble [5–9], as discussed further in Section 2. Wisselmann [10] conducted an analysis where the motorcycle stiffnesses were progressively eliminated (i.e., set to infinity); in this case also, a remarkable variation in the motorcycle response was shown.

For weave mode, the situation is different: the well-known correlation between eigenmode-damping and speed is also reproduced by models without chassis compliances [2,5,6]. In this case, up to a certain speed, the weave mode becomes more stable with increasing speed. After a tipping point, the stability degenerates again when the speed increases. This behaviour is unexpected, as the increasing gyroscopic moments of the wheel should stabilise the motorcycle, as is the case, for example, with a gyroscope. This is a complex system to analyse because there are many possible gyroscopic moments and their combined influence is not trivial. This peculiar behaviour is further analysed in Section 4.2.

The different models that will be presented within this paper were produced using open source multibody simulation software named “MBSim” (www.mbsim-env.de) which was developed at the Institute of Applied Mechanics of the Technical University of Munich. An introduction [11] on the functionalities of this software is provided. Multibody simulation is common for vehicle dynamics, and was used, for example, by Cossalter in multiple publications [2,5,7,12]. It allows the building of the desired model through a CAD-like interface, by connecting the bodies with joints and assigning them stiffness and damping when needed. The present motorcycle model is described in Section 3.

To summarise, this work deeply investigates the influence of the front fork bending compliance on the wobble mode. Starting from the point reached by previous authors [1,5,6], Section 4.1 provides a different justification for the well-known effect of the fork bending compliance on wobble damping. Moreover, in Section 4.2 the weave mode is further analysed and a possible justification for its damping behaviour is provided. Finally Section 4.3 investigates the influence of the rider on wobbling and weaving.

2. Related Work

Vehicle dynamics is a very popular research topic which features in many books and publications. Most of the literature is focused on four-wheelers; nevertheless, there is also a huge collection of research on two-wheeled vehicles. The different relevant authors are mentioned below.

Back in 1971, Sharp [3] published a paper about the driving stability of two-wheeled vehicles. This research is considered the starting point of the modern motorcycle dynamics. In fact, thanks to a (linearised) tyre model it was possible to detect the wobble mode, which was not present in the even earlier and less complex motorcycle models by Whipple [13] (p. 195).

Cossalter [2] (p. 278) [5] and Spierings [6] presented a solution to overcome the previously mentioned incoherence between reality and rigid model simulations when analysing wobble. A fork bending compliance with a lumped stiffness was added: a revolute joint in the front fork, with its rotating axis (named twist axis [14]) perpendicular to the steering head axis. A certain stiffness and a damping are assigned to this joint. Lumped parameter models are described in [15]. This kind of modelling is also found in other sources, especially when a more complex non-rigid model is developed [16–21].

This additional fork bending results in a more realistic wobble-damping characteristic: wobble-instability at low speed and a clear stabilisation when increasing the speed. Cossalter [2] (p. 280) and Spierings [6] explain this change of characteristic with the combination of two opposed effects caused by the fork bending compliance:

1. The bending compliance itself reduces the stability.
2. The combination of wheel-spin and the rotation around the twist axis produces a gyroscopic moment about the steering axis, leading to stabilisation.

Since the gyroscopic moment is proportional to the speed, the first effect dominates at low speed, causing lower stability in this speed range. The second effect becomes dominant with increasing speed, which explains the restored stability at high speeds. Section 4.1 investigates the influence of the fork bending compliance considering another phenomenon caused by the bending compliance itself.

There are several parameters affecting a motorcycle's wobble stability; a complete list can be found in [2,3,17,21]. For this work, besides the fork bending compliance, two tyre parameters are of particular importance: the relaxation length and the cornering stiffness. Some research [3,16,17,20] has underlined that a tyre model with cornering stiffness is necessary in order to simulate the wobble mode. This also suggests an important consideration: the principal cause of the wobble is given by the tyre's response. When the wheel is subject to an outer disturbance steering the wheel itself, the tyre reacts with a side force which, thanks to the mechanical trail, produces an aligning moment around the steering axis. When returning to the equilibrium position, the wheel starts oscillating about the steering axis, thereby triggering the wobble mode [22]. Depending on the speed of the motorcycle, this oscillation will diverge (unstable behaviour) or converge to the equilibrium (stable behaviour).

The other important tyre parameter influencing wobble is the relaxation length [3,13,23]. Several works [3,16,17,20,24] investigated its effect on wobble damping, underlying how the relaxation length destabilises the wobble mode, since it generates a delay between the wheel steering and the tyre-lateral force generation. As a consequence, Sharp [3] (p. 323) clarifies that both tyre sideslip and tyre relaxation properties are fundamental for a proper representation of a motorcycle's dynamic properties. Like most of the tyre parameters, the relaxation length also depends on several factors. Pacejka et al. [25] and Sharp [1] report that the relaxation length increases with increasing speed. Moreover, a dependence on the vertical load is present. A more recent paper by Sharp [12] proposes a tyre model based on the Pacejka magic formula [26] where dependencies on both speed and vertical load are reproduced. This model and the related parameters are also used in the present work.

In summary, some minimal requisites for a correct analysis of the wobble mode can be defined. Pacejka [26] and Doria [16] suggest that the tyre properties have the greatest influence on motorcycle stability. The Pacejka magic formula [26] coupled with a first order dynamic response, as described in the previous paragraph, is necessary in order to produce reliable wobble stability analyses [13] (p. 324). This tyre model allows an accurate description of the tyre forces and moments if the frequency of the external forces is lower than 15 Hz [13]; these conditions are generally satisfied for common stability analysis, therefore the magic formula is used in almost all the latest researches based on multibody analysis [2,7,12,27–29]. In addition to the tyre modelling, the lateral compliance at the front of the machine is necessary when simulating wobble [13,30]. This can be obtained with a bending compliance of the front fork [5–9], or by adding a lumped torsional stiffness of the main frame at the steering head joint with its rotation axis perpendicular to the steering axis [12,26–28]; a combination of both stiffnesses can also be implemented, as in the present work.

Besides the wobble mode, many of the mentioned sources also analyse vehicle "weave" [2,3,5–7,17,19,21]. The weave mode can also be qualitatively represented with a motorcycle model having no flexibilities [13] (p. 195). However, the literature underlines that some additional degrees of freedom (DoF) notably influence the weave mode. In particular, Doria [17] (p. 17) and Splerings [6] (p. 28) underline that the fork bending compliance destabilises the weave mode. Taraborrelli [23] and Cossalter [7] analyse the effect of the swingarm torsional and bending compliance. Reference [23] simulated two motorcycle types with significantly different stiffness values: a super-sport motorcycle (higher stiffness), where the two swingarm compliances had almost no influence on weave, and an enduro-motorcycle, where the swingarm bending compliance slightly destabilised the weave mode, which was at the same time slightly stabilised by the torsional compliance of the swingarm. The results of [7], on the contrary, show the destabilising effect of both swingarm bending and torsional compliance; however, the influence was also small in this case.

Furthermore, the rider has proven to greatly affect the motorcycle's stability behaviour. In fact, Roe [31] points out that the stability analysis of a riderless motorcycle can be very

misleading. Significant changes in the weave stability due to the rider have also been reported by Pacejka [26] (p. 535). The modelling of the rider's passive response and its influence on stability is a broad topic which will be summarised in Sections 3.3 and 4.3.

An interesting argument strictly connected to weave is the so called "cornering weave". During cornering, the in-plane eigenmodes (bounce, pitch) become increasingly coupled with the out-of-plane eigenmodes (weave, wobble), whereby the former shows degrees of freedom typical of the latter and vice versa [9,13,32]. Concerning cornering weave, the eigenvector also shows front and rear suspension travels which are not present in the straight-running weave [32]. This mode-coupling is critical because it provides a signal transmission path from road undulations to lateral motions [33]. Moreover, under cornering conditions, bounce and weave have similar eigenfrequencies in the middle to high speed range (70–120 km h⁻¹) [9,24,32,34], thereby leading to mutual triggering [13,33,34]. From these considerations it should be clear that the suspension system must also be modelled when carrying out stability analysis of motorcycles under cornering conditions [13,34].

As mentioned in the introduction, the models for the present work were implemented with the "MBSim" multibody simulation software. Two interesting references in this field are the works of moreCossalter [29] and moreLot [35]. They did not use the same software, but developed two multibody-simulation tools that follow the same principle; they are both based on the symbolic calculation software "Maple" with the second one using a build-in library for multibody modelling called "MBSymba". These references underline the suitability of a multibody simulation tool for the dynamics and stability analysis of motorcycles. Another piece of software used in several works [12,27,36] is "Autosim"; in this case as well, the authors demonstrated the great advantages provided by multibody modelling when conducting both time and frequency analyses. Following this established research, this modelling and calculation method were chosen for the present work.

3. Modelling

Different models have been developed during the last 70–80 years. Their complexity is obviously related to the objectives they pursue. For example, the wobble has been simulated studying systems capable of shimmy behaviour [37] (p. 166). Limebeer [13] (p. 184) derived the equations of motion of such a system, which possesses two DoF:

1. Rotation about the steering axis (in this case perpendicular to the ground).
2. Lateral translation of the steering joint used to reproduce lateral flexibility.

The model does not take into account the gyroscopic influences. A linear model with relaxation effect is used for the tyre forces. Even with this strongly simplified configuration, some important effects are described, which also occur in motorcycle modelling. The destabilising effect of the cornering stiffness, as prescribed by Sharp [3], is reproduced. Moreover, the inversion of behaviour experienced in motorcycle simulation when using an infinite stiff front frame (Section 2) is also present. This is a remarkable result, as this model does not reproduce the gyroscopic moments, which are considered in [2,6] as responsible for the inversion of behaviour. This could suggest that also other phenomena influence the wobble stability. In Section 4.1 this hypothesis is further developed.

Limebeer [13] (p. 189) carries on his analysis by converting the shimmy model into a front fork model. In this case, the caster angle is considered for the steering axis and the gyroscopic effects are also considered. Another important feature is a revolute joint connecting the fork assembly to the ground. This simulates the motorcycle's frame torsional flexibility, which provides a lateral flexibility at wheel level, as described in Section 2. Thanks to this feature, the eigenvalue analysis of this system provides results similar to those generally obtained with motorcycle modelling. Cossalter [2] (p. 251) also produced a similar model with the aim of studying wobble; however, it lacks the mentioned lateral flexibility and transient tyre properties, thereby failing to capture the physics of the wobble mode.

The simplified front fork model is acceptable when the aim is to only reproduce wobble. When studying weave, however, a whole motorcycle model is needed. The "basic" motorcycle model

- Swingarm torsion (α_{sw}), simulated with a revolute joint at the swingarm anchor point with rotation axis parallel to the main frame x axis.

The motorcycle parameters in [12] were obtained through experimental measurements or through estimates. However, some parameter variations have been used in the present work:

- The data for the rider's upper body mass and inertia tensor were taken from [12]. In [12] the mass and inertia tensor of the rider's lower body and of the motorcycle's main frame were fused together. In the present work, with the aim of allowing lateral translation of the rider's hip (considered as lower body in the present work), the mass and inertia tensor of the main frame in [12] were split between hip and main frame, while ascertaining that the combined inertia tensor and the overall centre of gravity remain unchanged. The data for hip's mass and inertia tensor were taken from [38]. According to these data, the mass and inertia tensor of the main frame were properly modified. In particular, the hip mass was subtracted from the main frame mass in [12]. Moreover, as explained above, the inertia tensor of the main frame was adapted so that the whole inertia tensor of the lower body and main frame together was equal to the main frame inertia in [12]. The rider's legs were considered fixed to the main frame, so their mass and inertia were included in it. As reported in [12] (p. 252), the rider's total mass was 72 kg.
- In the year of publication of [12] the experimental data of the front fork were not completely available. Some of them were judged by the authors of the present work as not realistic (for example, the mass of the lower fork and its lacking inertia tensor). For this reason, the front fork mass and inertia data were taken from [39], while retaining the overall geometry given in [12].

The motorcycle's parameters are reported in Appendix A.

The tyre forces and moments were reproduced with the Pacejka magic formula; further details on the tyre model are given in Section 3.4. The software for the motorcycle model is available on GitHub: https://github.com/TUMFTM/motorcycle_model.git.

3.2. Suspension

There are several types of motorcycle suspension. The simplest configuration is composed of a telescopic front suspension and a cantilever rear suspension. However, multi-link suspensions have been developed for both front and rear wheels. For the rear suspension, the multi-link solution allows a non-linear damping curve to be obtained even with a linear damper, as the kinematic function of the damper travel can be adjusted using a rocker. Multi-link at the front suspension generally increases the fork stiffness and favours the anti-dive property. For further details the reader is referred to [13] (p. 327). The motorcycle adopted in the present work uses a telescopic front suspension and a unitrack-like rear suspension (definition of [13]), where the spring-damper unit is connected to the chassis and to a rocker, while a pull rod connects the rocker to the swingarm. The kinematic functions of this rear suspension are presented in [12]. Figure 1 shows its geometry.

3.3. Rider Model

In contrast to cars, the rider's weight strongly influences the total motorcycle weight in riding conditions. Moreover, the rider has some relative motions with respect to the motorcycle. One can therefore expect the rider to have a great influence on motorcycle stability. This is indeed the case, as shown by both simulation [7,40] and experimental [41] results. In this work we only focus on the rider's passive motions. This is reasonable, as the eigenfrequencies of wobble and weave are too high for the rider to actively counteract them; therefore, it can be assumed that the rider behaves as a passive body when the motorcycle experiences wobble or weave. Under this assumption, different rider models can be developed. The most simple model has been adopted by several works [12,26–28] and includes only one DoF: the rider's upper body rotation about an axis parallel to the frame x axis. A different one-DoF model [42] reproduces the rider's rotation about the vertical axis (parallel to the frame z axis); moreover, the connection between the upper body and handlebar is included

with a parallel rotational spring-damper element. A 2-DoF model can then be obtained by combining the two previously described models [40]. Finally, the lateral displacement (frame y axis) of the rider’s hip can be added, thereby obtaining a 3-DoF rider model [7]. An interesting observation is made by Limebeer [13] (p. 326) about the influence of the rider’s parameters: he reports that the rider’s upper body parameters mainly influence the weave mode, while the lower body parameters have a greater effect on wobble. The literature also offers several examples of more complex rider models containing up to 28 DoF [43]. In this case, the rider model was used to faithfully evaluate the motorcycle race performances, so that the whole rider motion was needed, including his control action on the handlebars and his lean-in strategy. As introduced at the beginning of this paragraph, the current work pursues a very different objective, i.e., the analysis of the motorcycle eigenmodes, so that such a complex rider model is not necessary and would only complicate the interpretation of the results.

The rider model used in the present work is based on that presented in [7]. The rider is composed by two masses, representing the upper and lower body. The DoF are:

- α_{ri} : the rider’s upper body lean.
- γ_{ri} : the rider’s upper body yaw.
- y_{ri} : the rider’s hip (lower body) lateral motion.

As previously said, the connection with the handlebar is modelled by a rotational spring-damper element which reacts to the relative rotation between the upper body and handlebar, and applies equal and opposite moments for lower body and upper body, and frame and steering head, respectively.

3.4. Tyre Model

As introduced in Section 2, the present model uses the Pacejka magic formula to describe the tyre forces. The tyre model is analogous to that reported by Sharp [12] and is suited for motorcycles, as it accounts for the lateral force generation due to the wheel roll angle (camber angle). Moreover, it also describes the longitudinal forces, thereby allowing the motorcycle to be simulated in all possible conditions. Another peculiar factor is the description of the combined longitudinal and lateral force generation. This means that the maximal tyre-lateral force is reduced when the tyre simultaneously generates a longitudinal force (and vice versa). The model also takes into account the variation of the tyre potential with changing vertical load.

The present tyre model considers the tyre width. In this way, in contrast to thin disc models, the overturning moment must not be added separately, as the lateral migration of the contact point automatically generates this overturning moment [12,28].

The magic formula needs some inputs: longitudinal slip (κ), slip angle (α), camber angle (ρ_w), vertical load (F_z). κ can be calculated with Equation (1).

$$\kappa = -\frac{v_{x_C} - \omega_y (r_{rim} + r_c \cos \rho_w)}{v_{x_C}}, \tag{1}$$

where v_{x_C} is the longitudinal velocity of the tyre contact point, r_{rim} is the rim radius, r_c is the tyre crown radius and ω_y is the wheel rotation speed. α is calculated with a first order relaxation equation:

$$\frac{\sigma}{v_{x_C}} \dot{\alpha} + \alpha = \alpha_{ss}, \quad \alpha_{ss} = -\arctan \left(\frac{v_{y_C}}{v_{x_C}} \right), \tag{2}$$

where α_{ss} is the slip angle in steady-state conditions, while v_{y_C} is the lateral velocity of the tyre contact point. This means that the lateral force due to the slip angle is generated with some delay depending on the relaxation length σ . Its value is not constant and depends on both longitudinal speed and vertical load; these dependencies are taken into account in the present model. The longitudinal force and the lateral force due to the camber angle are assumed to build up instantaneously, so no relaxation equation is used.

At this point, a geometrical model of the tyre contact point and a related reference frame are needed in order to calculate the velocity components v_{y_C}, v_{x_C} at the contact point itself and the vertical load F_z . Firstly, the orientation of the reference frame at the contact point has to be obtained. It should satisfy the following requirements: z axis being perpendicular to the road; x axis being in the wheel plane and parallel to the road. Such a reference frame can be derived with two rotations starting from the reference frame of the wheel carrier, indicated in the following with the subscript W_c . The intermediate reference frame W is obtained as follows:

$$\begin{aligned} W e_x &= \frac{W_c e_y \times I e_z}{|W_c e_y \times I e_z|}, \\ W e_y &= W_c e_y, \\ W e_z &= W e_x \times W e_y, \end{aligned} \tag{3}$$

where ${}_{ref}e_i$ is the unit vector of the i th axis of the reference frame named "ref", and $I e_z = [0, 0, 1]^T$. The frame W has the x axis parallel to the ground. In order to get C , another transformation is needed, which allows the z axis to be perpendicular to the ground:

$$\begin{aligned} C e_x &= W e_x, \\ C e_z &= I e_z, \\ C e_y &= C e_z \times C e_x. \end{aligned} \tag{4}$$

The unit vectors in Equation (3) define the rotation matrix ${}_I S_W = [W e_x, W e_y, W e_z]$ from frame W to the inertial frame I . Similarly, the rotation matrix from frame C to I is defined as ${}_I S_C = [C e_x, C e_y, C e_z]$. Now the longitudinal and lateral velocities v_{x_C}, v_{y_C} can be calculated in the following steps:

$$\begin{aligned} {}_W v_{W_c} &= {}_I S_W^T {}_I v_{W_c}, \\ {}_W v_C &= {}_W v_{W_c} + {}_W \omega_{W_c} \times [0, -r_c \sin \rho_w, -r_{rim} - r_c \cos \rho_w]^T, \\ {}_I v_C &= {}_I S_W {}_W v_C, \\ {}_C v_C &= {}_I S_C^T {}_I v_C. \end{aligned} \tag{5}$$

${}_B v_A$ is the absolute velocity vector of the generic point A in the generic frame B . The vector ${}_C v_C$ represents the velocity of the contact point in frame C ; its first and second components provide v_{x_C}, v_{y_C} .

The last remaining input for the magic formula is the vertical load. This is composed by a constant $F_{z,stat}$ and a varying part $F_{z,dyn}$. The constant one is obtained in static equilibrium conditions. The second one depends on motorcycle trim and can be calculated using the tyre carcass compression Δz_{tyre} from the nominal state.

$$\Delta z_{tyre} = -r_{rim} \cos \rho_w - r_c + {}_I z_{0C} - {}_I z_{W_c}. \tag{6}$$

${}_I z_{0C} > 0$ is the vertical distance under static equilibrium conditions between the origin of the inertial frame I and the contact point. ${}_I z_{W_c} > 0$ is the instantaneous vertical distance between the origin of the inertial frame I and the wheel carrier W_c . Finally, the tyre vertical load F_z is calculated as follows:

$$F_z = F_{z,stat} + F_{z,dyn} = F_{z,stat} - c_z \Delta z_{tyre} - d_z v_{z_C}. \tag{7}$$

c_z, d_z are the tyre vertical stiffness and damping, respectively. It is worth pointing out that Δz_{tyre} is negative when the carcass is compressed; therefore, the carcass compression leads, through Equation (7), to an increased vertical load.

All the inputs for the magic formula are now available. The equations of the magic formula are taken from [12], so they are not repeated here. The outputs are: longitudinal force, lateral force and aligning moment. These outputs are applied in the wheel carrier and not at the contact point as in [12]. This choice was made because in MBSim the forces must be applied to a body, which would require the definition of a body in the contact point, which in the actual model structure is not an easy task. Shifting the tyre forces in the wheel carrier requires applying additional moments; this is, however, easily done, as all the lever arms are known or can be derived with geometric reasoning. The equivalence between this force system and the one with the forces applied at the contact point has been verified on a simplified model with a single wheel. The results are equivalent, thereby confirming the correctness of the choice made.

3.5. Validation

As explained in Section 3.1, the motorcycle model in the present work is based on the data of [12]. The obvious solution is then to validate the present model against this reference by Sharp. In order to do so, the front fork data were set to the values in [12]; moreover, the additional DoF were "switched off." This was possible thanks to a functionality developed for this purpose in MBSim, which allows the selection of the DoF to be considered. Reference [12] reports the simulation results of a steady-state cornering condition with fixed roll angle and at different speeds. Several variables are then shown under this condition; particularly important for steady-state cornering are: steering torque, front and rear tyre-lateral forces and aligning moments. The same condition has been tested in the present work and the variables compared. The accordance is very good, with deviations less than 5% for all values. This is shown Figure 2, where F_{y_f} , F_{y_r} are the front and rear tyre-lateral forces, while M_{z_f} , M_{z_r} are the front and rear tyre aligning moments and T_δ is the steer torque.

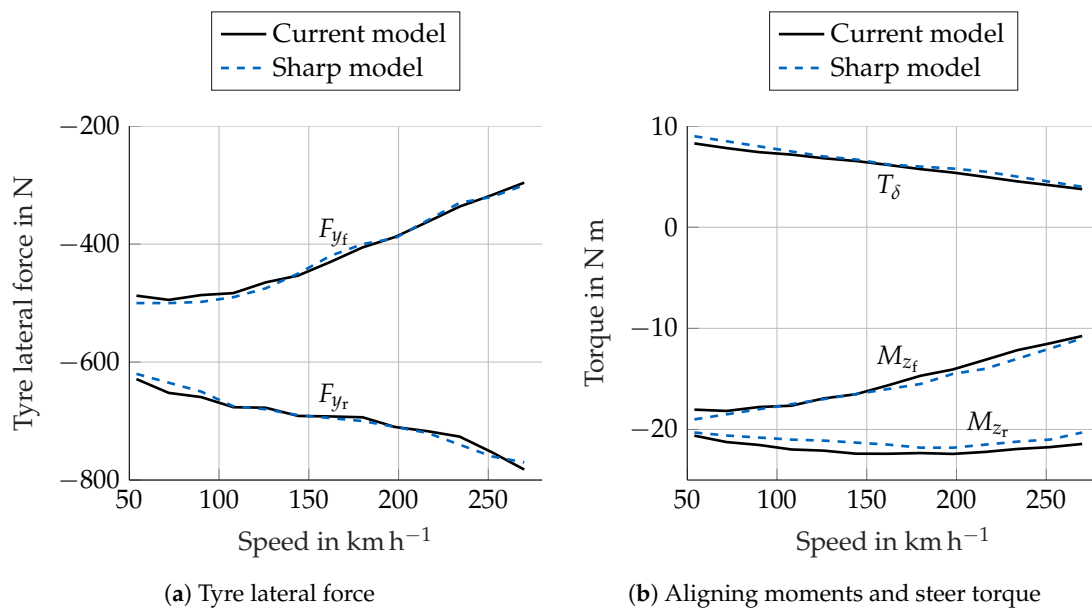


Figure 2. Model validation with steady-state analysis: comparison between the current model and the model of Sharp for a steady-state cornering maneuver. F_{y_f} , F_{y_r} are the front and rear tyre-lateral forces, while M_{z_f} , M_{z_r} are the front and rear tyre aligning moments and T_δ is the steer torque.

As further validation, the present model was also compared with that in [26] (p. 508) by Pacejka. This model renounces some DoF with respect to [12]: the suspensions are not modelled. Moreover, the frame torsional stiffness is not present, while the front fork has bending compliance. Using the same data of [26] and with the same DoF, a comparison of the eigenvalue analysis has been carried out. Additionally, in this case the agreement of the results is very good, with the curves of the wobble

and weave eigenfrequencies and damping as a function of the speed almost overlapping, as shown in Figure 3. In this figure, the frequency is expressed in rad s^{-1} in order to facilitate the comparison with the results of [26], where this unit of measurement is used. In the subsequent paragraphs, however, the frequency will be expressed in Hz. Additionally, the selection of the speed range in Figure 3 was made according to [26].

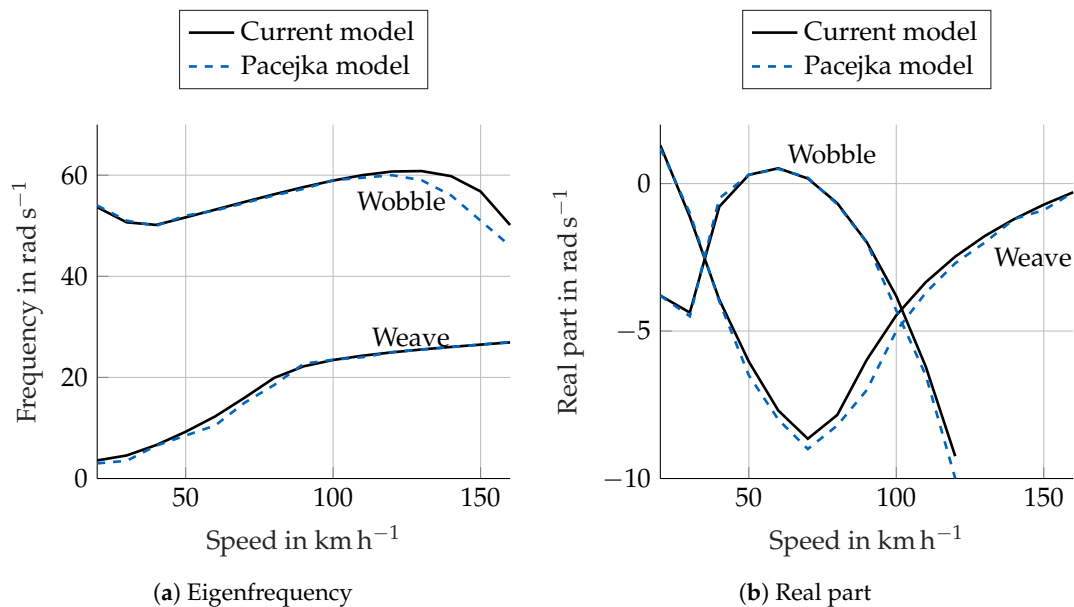


Figure 3. Model validation with eigenvalue analysis: comparison between the current model (parametrised with the same data of the Pacejka model) and the model of Pacejka.

4. Results

This section shows the eigenvalue analysis and the time response for the presented model. Starting from these plots, some physical relations will be derived and will help to understand the important phenomena influencing the behaviour of the wobble and weave eigenmodes as a function of vehicle speed.

4.1. Wobble

Section 2 describes how the front fork lateral flexibility (bending-compliance about the x axis) strongly influences the stability of wobble. This difference is shown in Figure 4. In order to isolate the influence of the fork compliance, the curve relative to the rigid fork was obtained with a 9-DoF model, wherein the DoF used to represent the motorcycle's stiffnesses, as described in Section 3.1, have been eliminated. Moreover, the rider's DoF are not present. In the curve relative to the flexible fork, only the DoF α_{ff} has been added, so that the DoF are 10 in total. With the parameter set used in the present work and in the speed range considered, the wobble mode remains well damped. This is due to the relatively high value of the steering damper. In the following part of this section, the reason for such a drastic behaviour change between rigid and flexible fork is addressed. In particular, a possible cause is presented which partially differs from the explanation provided by Cossalter [2] (p. 280) and Spierings [6].

A key concept described in Section 2 is the correlation between tyre properties and wobble. In particular, a tyre model with cornering stiffness is necessary to reproduce wobble [3,16,17,20]. Therefore, the tyre and specifically the lateral force due to the slip angle is a fundamental factor when considering wobble stability. However, what is the reason for the behaviour inversion in Figure 4 and how can it be attributed to the tyre response? Equation (2) shows how the slip angle depends on the

lateral velocity of the wheel contact point v_{yC} . The fork lateral flexibility allows some lateral motion of the wheel because of the rotation about the revolute joint axis (fork x axis), thereby influencing v_{yC} .

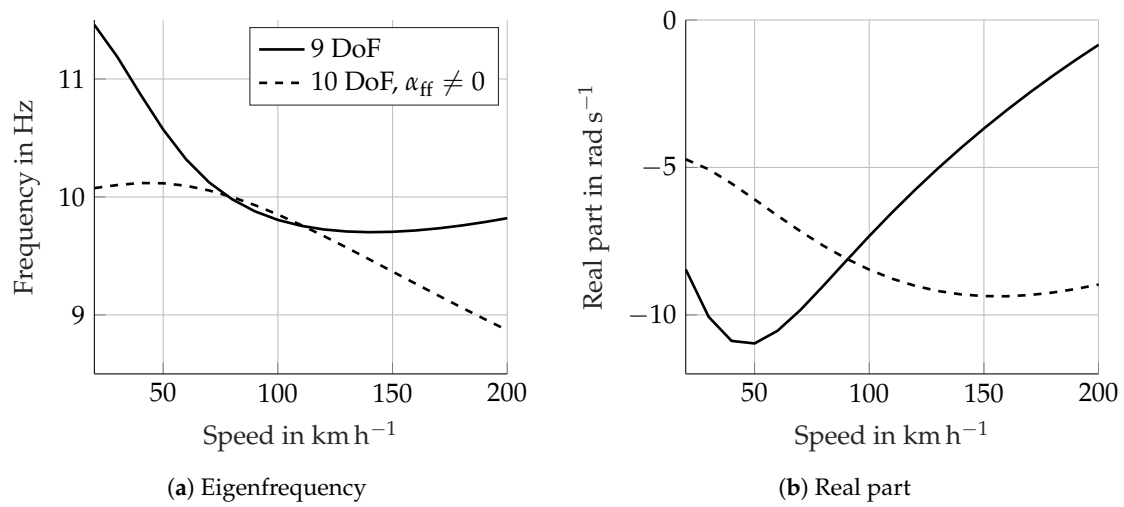


Figure 4. Influence of front fork flexibility on wobble.

This concept is shown schematically in Figure 5. The variation of v_{yC} due to the fork lateral flexibility can be expressed as:

$$\Delta v_{yC} = h \dot{\alpha}_{ff}. \tag{8}$$

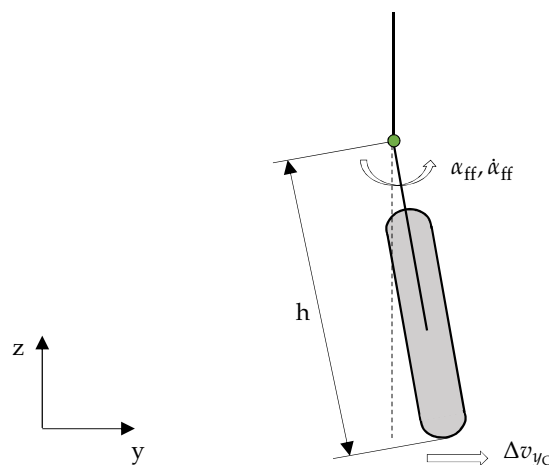


Figure 5. Variation of the lateral velocity at the contact point due to lateral fork flexibility.

To prove the effect of Δv_{yC} , it is compensated by subtracting its value from v_{yC} in Equation (2). Figure 6 shows the corresponding eigenvalue analysis with the dots-marked curve. The compensation of Δv_{yC} remarkably stabilises wobble. Moreover the curve shows the same behaviour for the 9-DoF model. At this point a conclusion can be drawn: the fork lateral flexibility influences the wobble stability through its effect on the lateral velocity v_{yC} of the contact point.

In a subsequent step, it is of particular interest to observe whether Δv_{yC} increases or reduces the value of v_{yC} . Figure 7 shows a time simulation at 50 km h⁻¹ with a steer torque impulse as excitation. The full line represents v_{yC} obtained from Equation (5); the dashed line was obtained with $v_{yC} - \Delta v_{yC}$, whereby Δv_{yC} was derived from Equation (8). The subtraction of Δv_{yC} increases the value of v_{yC} : Δv_{yC} , which is normally included in v_{yC} , thereby reduces the amplitude of v_{yC} . The tyre-lateral force is proportional to the slip angle, which is proportional to v_{yC} (Equation (2)). This force tends to

oppose the wheel motion due to the wobble oscillation. Therefore, the fork flexibility introduces a Δv_{yC} , which reduces the tyre-lateral force. This explains why the curve with $\Delta v_{yC} = 0$ in Figure 6 is significantly more stable than the 10-DoF case with $\Delta v_{yC} \neq 0$.

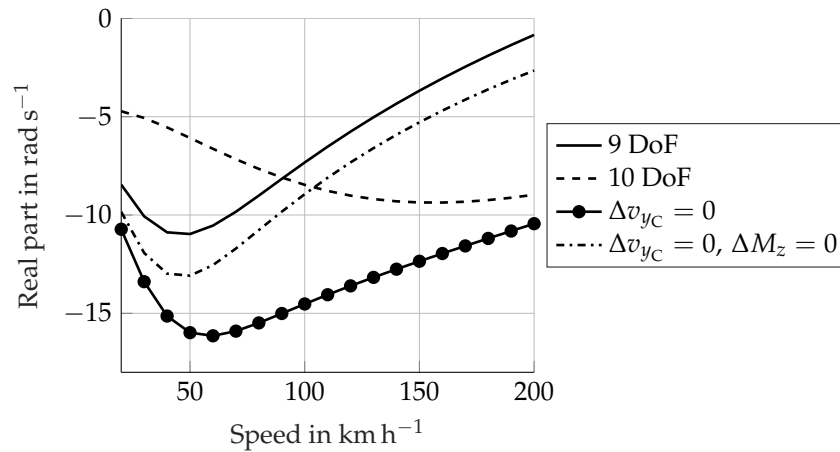


Figure 6. Effect of compensating Δv_{yC} on wobble damping. In the dotted curve only Δv_{yC} is compensated. In the dash-dotted curve both Δv_{yC} and ΔM_z (with Equation (9)) are compensated.

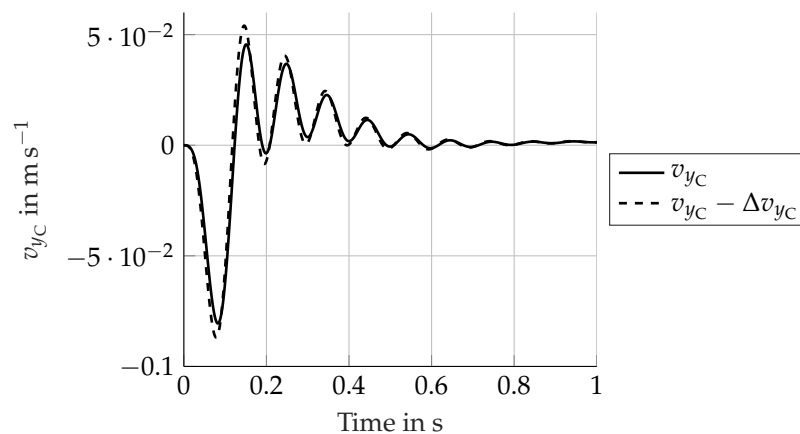


Figure 7. Variation of the lateral velocity of the contact point v_{yC} due to front fork flexibility. Time simulation at 50 km h⁻¹ and with a steer torque impulse as excitation.

Even if the curve with compensated Δv_{yC} in Figure 6 assumes the same qualitative behaviour as the 9-DoF model, the damping values are still significantly different. In order to get a curve similar to that of the 9-DoF model, the gyroscopic moment introduced by fork bending must be compensated. The moment acts about the steering axis and can be calculated with Equation (9) (this formula differs from the complete Euler equations (compare to Equation (10)), whose left-hand side defines the whole gyroscopic effects. Equation (9) is used here because its simple structure allows one to compensate the gyroscopic effects about the steering axis as external moments in the used multibody simulation software), as shown by Cossalter [5]. This formula is also well-known in the literature, as it is present in the book on vehicle dynamics by Mitschke [44]. The symbol Δ in Equation (9) indicates that the formula only refers to the gyroscopic moment due to the fork lateral flexibility.

$$\Delta M_z = \dot{\alpha}_{ff} \omega_{y_{fw}} I_{y_{y_{fw}}}, \tag{9}$$

where $\omega_{y_{fw}}$ is the front wheel rotation speed and $I_{y_{y_{fw}}}$ is its polar moment of inertia. The dash-dotted curve in Figure 6 shows the effect of compensating ΔM_z . As expected, the damping curve gets very

close to the 9-DoF model. The remaining offset can be attributed to other secondary phenomena, which have not yet been completely identified.

In summary, the influence of the fork bending compliance on wobble can be explained by considering two main phenomena:

1. Gyroscopic moment;
2. Variation of the lateral speed of the wheel contact point.

Both of them originate through the rotation α_{ff} and its time derivatives.

When observing the curve of the 10-DoF case in Figure 6, it is evident that it is less stable than the 9-DoF case only up to about 80 km h^{-1} . Above this speed, the higher stability of the 10-DoF model compared to the 9-DoF model can be justified with the same consideration made by Cossalter [5]: the gyroscopic moment ΔM_z about the steering axis stabilises the wobble with increasing speed.

At this point another question may be raised: Which phenomenon is responsible for the decreasing wobble damping shown by the 9-DoF model and the model with compensated Δv_{yC} compared to the 10-DoF one? To answer this question, a model containing only the front fork and front wheel has been used. With this model two cases are studied: two DoF characterised by the rigid fork and three DoF with a flexible fork; the first model correlates with the 9-DoF model, and the second with the 10-DoF model.

Figure 8a shows the damping curves for these two models. Different variations were made: the wheel inertia tensor I_{fw} was set to 1% of the original value (to eliminate the gyroscopic moments) and Δv_{yC} has been compensated as in Figure 6. Some important conclusions can be drawn:

- The 2-DoF model did not show a decrease in damping with increasing speed, as did the 9-DoF model.
- The damping of the 3-DoF model grew more rapidly than the one of the 10-DoF model.
- The case $I_{fw} = 1\%$, $\Delta v_{yC} = 0$ is very close to the curve of the 2-DoF model, as was expected by theoretical observations. In fact, the 2-DoF model had no gyroscopic moments about the steering axis, as no rotation about the fork x axis was present. In Figure 6 the curve with $\Delta v_{yC} = 0$ shows a remarkable offset compared to the 9-DoF curve because of the gyroscopic moments. With I_{fw} set to 1% they almost vanish, resulting in a smaller offset.

The difference in behaviour between the 2 and 9-DoF models can be justified by the additional roll motion of the 9-DoF case. This motion produces additional gyroscopic moments which apparently destabilise the wobble with increasing speed. These moments are also clearly present in the 10-DoF model. However, in this case they are compensated by the gyroscopic moment produced by the fork flexibility. The opposition of these two effects is underlined by the saturation shown in the 10-DoF model at about 150 km h^{-1} , which is not present in the 3-DoF model.

In summary, the wobble damping behaviour of a real motorcycle is determined by three principal mechanisms. The front fork flexibility produces a lateral movement of the front wheel, which can be represented with a rotation α_{ff} . This reduces the tyre-lateral force and thus decreases the wobble damping at low speed compared to a rigid fork. When the speed increases, the gyroscopic moment caused by the rotation α_{ff} increases in magnitude and stabilises the wobble, thereby making the 10 DoF model more stable than the 9-DoF model. The third mechanism is related to the gyroscopic moments caused by the motorcycle's roll motion. They destabilise the wobble with increasing speed, thereby explaining why the wobble damping in the 9-DoF model decreases with increasing speed. This does not happen in the 10-DoF model because the stabilising gyroscopic moment caused by α_{ff} outweighs the destabilising effect.

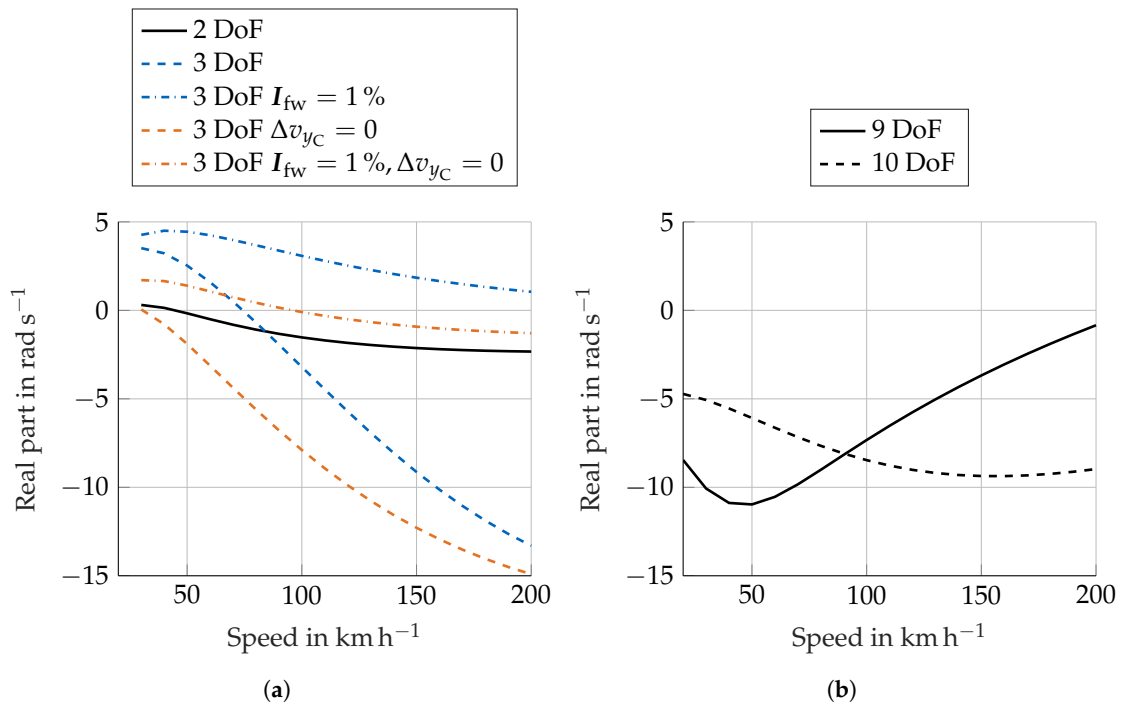


Figure 8. (a) Wobble damping for the 2 and 3-DoF models with variation of the tensor I_{fw} and compensation of Δv_{yC} . The curve with $I_{fw} = 1\%$ for the 2-DoF model is identical to that with $I_{fw} = 100\%$ so it was not plotted. (b) Figure 4b copied to facilitate the comparison.

4.2. Weave

The weave mode was already captured in its essence by the very first motorcycle model by Whipple [13] (p. 195). Moreover, there is no evidence of parameters which produce a behaviour inversion of the damping curve, as can be observed for the wobble mode. This already suggests that the weave mode reproduces in some way the "basic" motorcycle behaviour. This idea was also proposed by Schröter [45] (p. 28), who describes the weave mode as a degenerated dynamic stabilisation process involving steering, roll and yaw oscillations. This can be shown with a simple time simulation where the upright riding motorcycle is excited with a lateral force impulse applied to the frame. Assuming that the wobble is well damped, the motorcycle reacts to this excitation with a weave oscillation, which may diverge or stabilise depending on the motorcycle's speed and parameters.

Figure 9 shows the frequency and damping of the weave mode as a function of the speed. The effect of the rider is analysed in Section 4.3, so this figure refers to the case with a rigid rider; the other DoF are all present. In order to represent the saturation shown by the damping curve at high speed, the speed range differs from the one in Figure 4. The behaviour of the weave damping shows some interesting characteristics: below 70 km h^{-1} weave is stabilised with increasing speed; above it is destabilised. However, above 220 km h^{-1} the weave damping shows a plateau. This particular behaviour suggests that the weave mode changes with speed. Moreover, the speed dependency could be explained by a certain influence of the gyroscopic effects, which are also speed dependent. The gyroscopic effects are obtained with the whole left-hand side of the Euler equations, which is shown in Equation (10) for the front wheel.

$$I_{fw}\dot{\omega}_{fw} + \omega_{fw} \times (I_{fw}\omega_{fw}) = M_{ext}, \quad (10)$$

where ω_{fw} is the rotational velocity vector of the front wheel and I_{fw} is the front wheel inertia tensor.

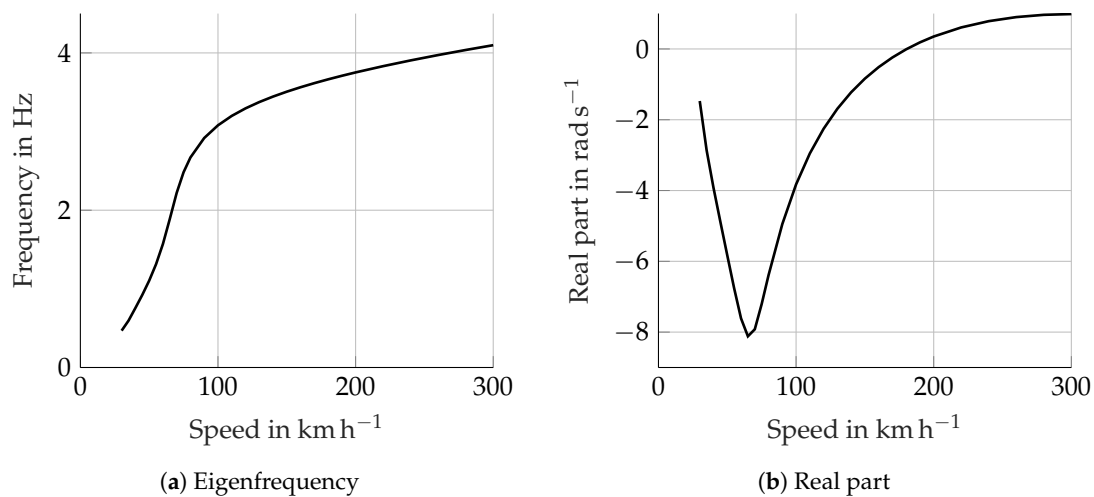


Figure 9. Weave eigenfrequency and damping as a speed function.

Figure 10 further illustrates this concept. In this figure, the weave eigenvector is shown with the so-called compass plot. The arrows are named phasors and represent how the motorcycle’s DoF are involved in the weave oscillation. An arrow’s length is the magnitude of the motion of the related DoF. In order to maintain the information about the absolute amplitude of the phasors, no normalisation is present. The phasor’s angle shows the phase. In the following paragraphs the relative angle between the phasors is called relative phase.

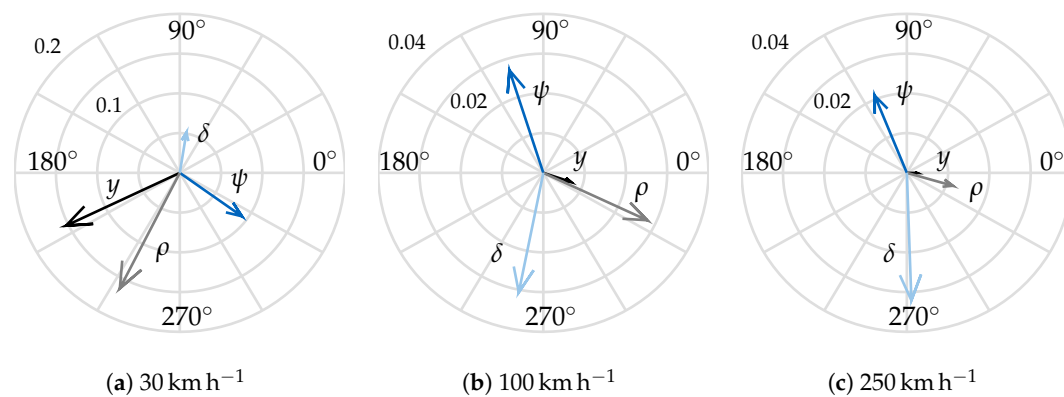


Figure 10. Compass plot of the weave eigenvector at different speeds. δ is the steering angle, ψ is the yaw angle, ρ is the roll angle and y is the lateral displacement.

At low speed, (Figure 10a) the roll (ρ) and lateral displacement (y) show big amplitudes. The latter is due to the small gyroscopic effects, so that if weave is excited (for example, with a lateral impulse), the motorcycle describes a “slalom” at low frequency (see Figure 9) involving a significant lateral displacement. This can be described as a low-frequency “self-stabilising” motion, which the literature already considers as weave.

As the speed increases (Figure 10b), the relative phase between the motions significantly changes, whereby the lateral displacement is no longer important. The other DoF show a similar amplitude. Finally, when the speed increases further (Figure 10c), the relative phase does not change remarkably. The most important observation, however, is the reduction of the roll (ρ) amplitude with increasing speed, which can be seen when comparing the related phasor in Figure 10b,c. This can also be observed in the time simulation. If the motorcycle is excited by a lateral impulse at high speed, the resulting weave oscillation does not show a significant roll motion, while the front wheel and the frame rotate

around the steering and vertical axis almost in opposition of phase, as shown by the vectors δ, ψ in Figure 10c. The reduction in roll motion with increasing speed is also shown by a free rolling wheel. This phenomenon can be explained considering the gyroscopic effects which increase with speed, thereby preventing the wheel (or the motorcycle) capsizing.

Which are the possible causes of the peculiar damping behaviour shown in Figure 9b? Some useful knowledge can be derived by an eigenvalue analysis with reduced wheel inertia. The correlation to Figure 10 is shown in Figure 11, for which the total wheel inertia tensors I_{fw}, I_{rw} was set to 10% of the original tensors. The first consideration resulting from the comparison is that in Figure 11 the relative phase between the phasors no longer changes with speed, as it happens in Figure 10. The plot at 30 km h^{-1} is not present, as the weave mode is no longer available at this speed. It is important to point out that, because of this massive inertia reduction, the gyroscopic effects almost disappear. Two main observations can be made:

1. The missing weave mode at low speed can be attributed to the (almost) missing gyroscopic effects. The time simulation at 30 km h^{-1} with a lateral force impulse shows that the motorcycle does not react to the excitation with a weave oscillation, but it capsizes. With the original inertia values the gyroscopic effects are present, despite the low speed. They prevent the motorcycle from capsizing immediately after the excitation and producing the low-frequency “self-stabilising” motion.
2. The gyroscopic effects are also the main cause for the change in the weave eigenvector shown in Figure 10. In fact, when they are very small, as in Figure 11, the relative phase between the eigenvector components is no longer speed dependent.

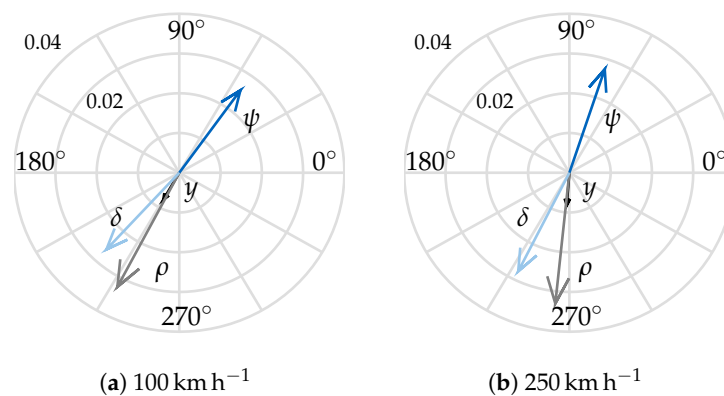


Figure 11. Compass plot of the weave eigenvector at different speeds with $I_{fw}, I_{rw} = 10\%$.

The correlation with Figure 9 is shown in Figure 12. The speed range starts now from 80 km h^{-1} , as for the following reasoning only this range is necessary. Moreover, the weave with reduced wheel inertia is not present up to about 50 km h^{-1} and in the range $50\text{--}80 \text{ km h}^{-1}$ it is extremely well damped (real part $> 25 \text{ rad s}^{-1}$). Similarly to the full inertia case, the damping continues to decrease with increasing speed in the small inertia case shown in Figure 12b. As the gyroscopic effects are almost missing, the reason for this behaviour can be determined by investigating in the tyre response. The tyre-lateral force is proportional to the slip angle which is in turn proportional to the ratio between v_{yC} and v_{xC} (Equation (2)). The authors verified that v_{yC} mainly depends on the kinematic steering angle (see [2] for its definition), which is proportional to the steering angle. Figure 11 shows that above a certain speed (100 km h^{-1}) the amplitude of steering motion in the weave eigenvector remains fairly constant. The numerator of α_{ss} in Equation (2) is therefore almost constant with speed. The denominator of α_{ss} is given by v_{xC} , which clearly increases with speed. As a result, α_{ss} decreases with increasing speed and so does the tyre-lateral force. The tyre-lateral forces tend to bring the motorcycle back to the equilibrium position, thereby stabilising the weave. The decreasing tyre force is therefore responsible for the decreasing weave damping and the hyperbolic behaviour of the dashed curve in Figure 12b.

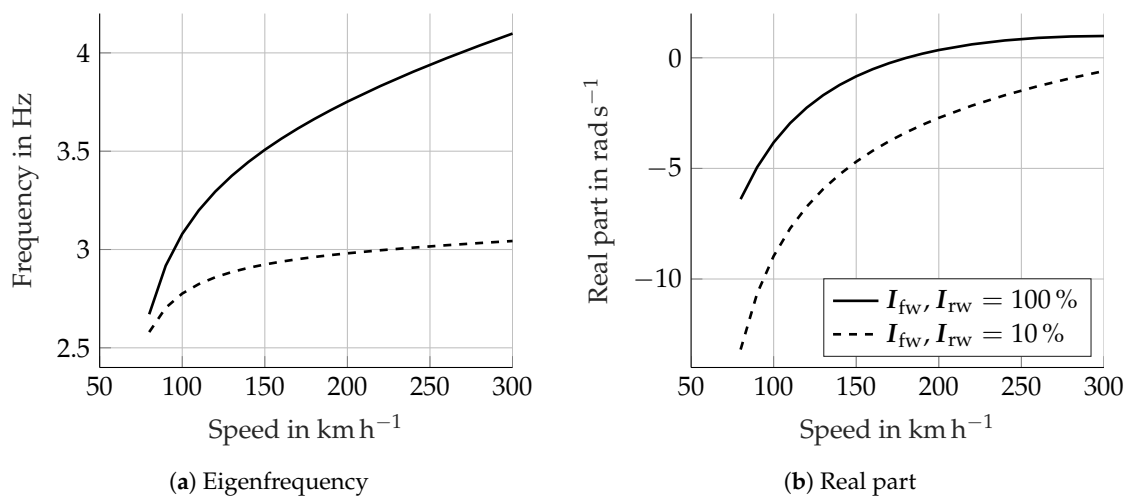


Figure 12. Comparison between the eigenvalue analysis with original wheel inertia tensors and reduced inertia tensors.

Considering again the curve with the original wheel inertia in Figure 12, the first observation is the smaller weave damping. This can be explained by taking into account the additional impact of the gyroscopic effects. The gyroscopic effects of the front wheel about the steering axis are in counterphase with respect to the tyre moments, as Figure 13 shows, therefore they work against them. For this reason, the weave damping is lower compared to the reduced inertia case. The gyroscopic effects also justify the slower damping decrease in the case with original wheel inertia (see Figure 12). In fact, due to the progressively changing eigenvector (Figure 10), i.e., the decreasing roll motion amplitude, the gyroscopic effects increase underproportionally with the speed. For example, in a time simulation with lateral force excitation, the first peak of the front wheel gyroscopic effects about the z axis increase from 100 to 150 km h^{-1} by 37.5%, while they only increase by 14.5% from 250 to 300 km h^{-1} . As a consequence, they also underproportionally reduce the tyre forces with increasing speed. This, combined with the decreasing tyre forces, leads to the mentioned saturation above 220 km h^{-1} , which is not present in the reduced inertia case.

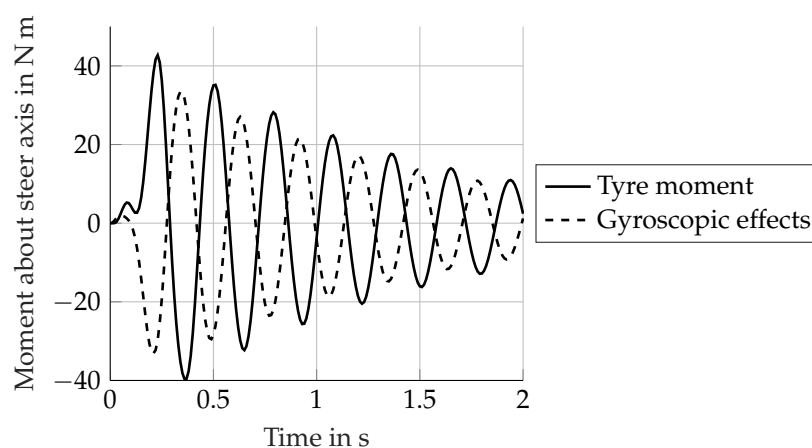


Figure 13. Front wheel gyroscopic effects and tyre moments about the steering axis. The time simulation was obtained with a lateral force excitation on the motorcycle frame at the speed of 150 km h^{-1} .

The last characteristic to be observed is the increase in damping shown below 80 km h^{-1} in Figure 9b. The authors’ belief is that in this lower speed range the weave mode can still be seen as the already mentioned low-speed “self-stabilising” motion. When increasing the speed, this motion progressively changes to the “real” weave, thereby producing the observed increase in damping.

Figure 14 illustrates this fact. Following the three compass plots with increasing speed, one can see that the phase and amplitude of the phasors progressively change; i.e., the weave changes from the “self-stabilising” motion to the classical weave. In fact, above 100 km h^{-1} the relative angle between the phasors no longer changes significantly, as the comparison of Figure 10b,c shows.

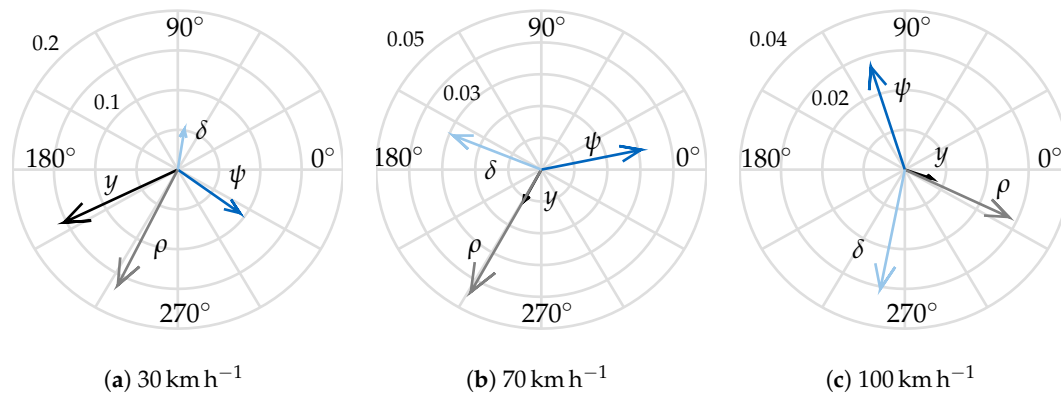


Figure 14. Compass plot of the weave eigenvector at different speeds.

4.3. Rider Influence

As explained in Section 3.3, the literature offers different examples of rider modelling. These references often analyse the influences of the rider on weave and wobble stability. For example, reference [42] investigates the effect of the rider yaw combined with the connection to the handlebar. Reference [7] proposes the eigenvalue analysis with the 3-DoF rider also used in the present work. In order to obtain a better overview of the single influences, this section aims to briefly summarise the essential differences between the three different DoF models used for rider modelling. This is shown in Figure 15. The effect of the single DoF can be summarised as follows:

- The rider lean α_{ri} stabilises the weave and destabilises the wobble at high speed. The increased stability of weave is a reasonable result because during the weave oscillation the rider lean is almost in counterphase to the motorcycle’s roll [41], thereby damping out this motion.
- The rider yaw γ_{ri} combined with the connection to the handlebar destabilises the weave, massively stabilises the wobble and also increases its eigenfrequency. This is in accordance with [42] and is a reasonable result, as the connection acts in a similar way to a steering damper, which also stabilises the wobble while destabilising the weave.
- The rider’s hip lateral motion y_{ri} hardly affects the eigenmodes, as also reported by [31]. The only remarkable influence is the increase in the wobble frequency at high speed.

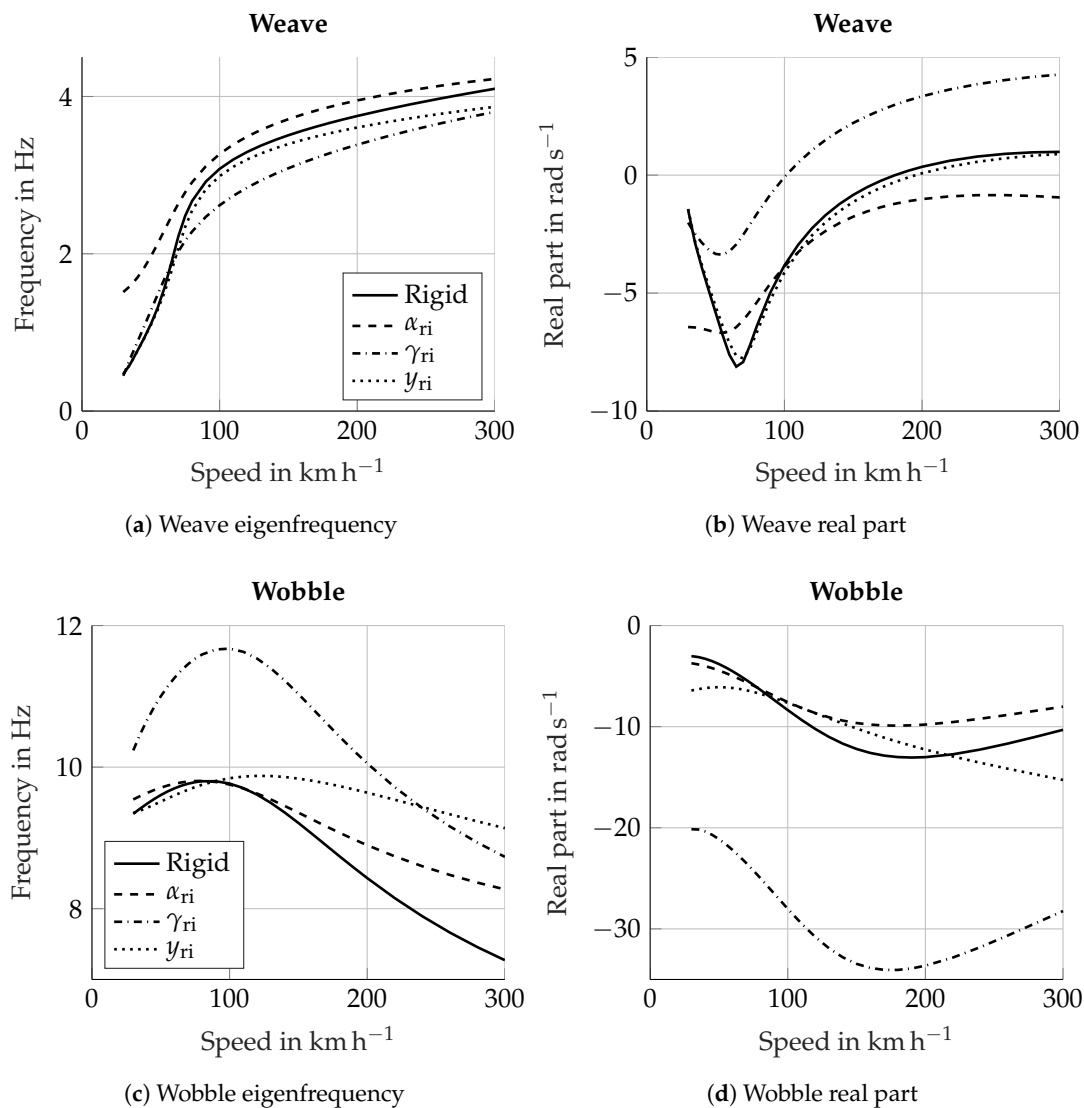


Figure 15. The effects of the single rider’s DoF on the weave and wobble modes.

Figure 16 shows the effect of the whole rider model, containing the three DoF α_{ri} , y_{ri} , γ_{ri} . In the weave the effect of α_{ri} overcomes the others, thereby causing the already mentioned stabilisation at high speed. When concerning wobble, the effect of γ_{ri} and the connection with the handlebar are dominant, leading to an increase in both frequency and damping.

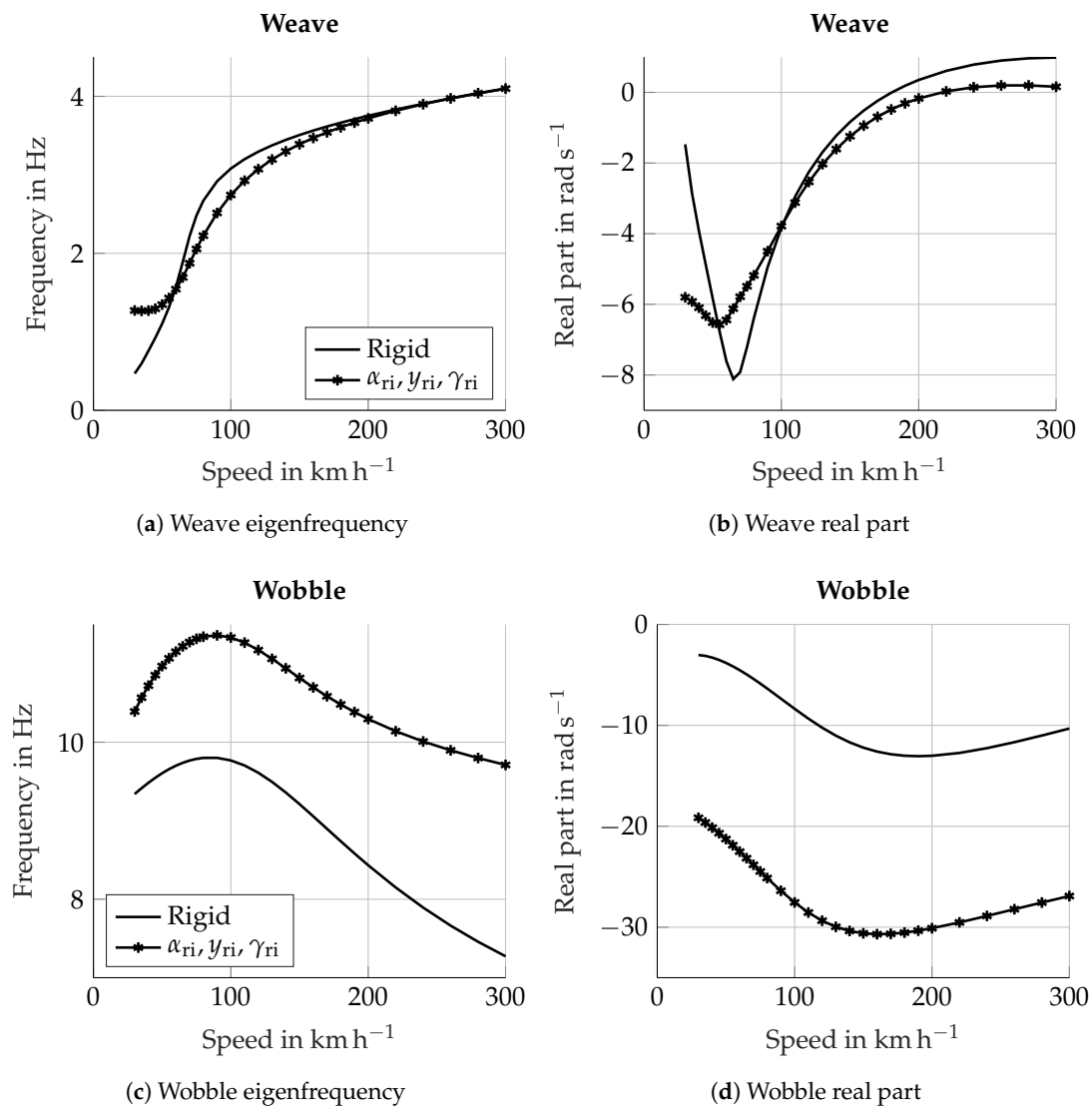


Figure 16. Effect of the whole rider model (3-DoF) on the weave and wobble modes.

5. Conclusions and Outlook

The present work further analysed the physical phenomena behind the wobble and weave eigenmodes. In particular, the effect of the front fork bending compliance has been discussed and a possible justification for the well-known weave damping behaviour with increasing speed is provided. Finally, the effect of the single rider’s DoF on the weave and wobble mode has been shown.

The first aspect has been addressed before by Cossalter [5] and Spierings [6]. They noticed that the modelling of the fork bending compliance allows very similar results to the real driving experience to be obtained: the wobble mode is unstable at low speed and stabilises with increasing speed. Without this parameter, the simulation results are not realistic. Cossalter [5] justifies this behaviour considering the superposition of two effects, both caused by the fork bending compliance: this compliance alone is destabilising but it also produces a gyroscopic moment about the steering axis that stabilises the wobble. The first effect dominates at low speeds, while the second prevails at high speed. The present work provides an additional perspective for explaining the effect of the fork bending compliance, though maintaining the validity of the previous results [5]. The additional insight is given by the tyre behaviour. It was demonstrated that the lateral motion of the wheel contact point caused by the fork bending compliance reduces the lateral component of the contact point velocity

v_{yC} . The tyre-lateral force is proportional to this velocity component through the slip angle. Reducing v_{yC} also reduces the tyre force. This causes a reduction in the wobble damping at below 80 km h^{-1} . At higher speeds, the effect of the gyroscopic moments introduced by the fork flexibility leads to increasing wobble damping with increasing speed, as explained by Cossalter [5].

The weave damping behaviour is well-known and involves a progressive stabilisation up to about 80 km h^{-1} (with the present parameters), then the damping decreases with increasing speed until it reaches a saturation above 220 km h^{-1} . This peculiar behaviour can now be explained. The weave eigenvector changes with speed. In the lower speed range this corresponds to a change from a low frequency self-stabilising motion involving a lot of frame lateral displacement to a weave oscillation where the lateral motion is no longer significant. The eigenvector change is supposed to be the main cause of the damping increase below 80 km h^{-1} . Above this lower speed range, the weave eigenvector does not change in the relative phase between phasors, but the roll component becomes progressively smaller. This influences the gyroscopic effects, which underproportionally increase with speed, thereby causing the plateau above 220 km h^{-1} .

The multibody model used in this work was provided with a functionality to select the different DoF. This gives the chance to investigate the separated influence of the single DoF used in the rider model. In particular, the rider lean stabilises the weave and slightly destabilises the wobble; the rider yaw plus the connection with the handlebar destabilises the weave and remarkably stabilises the wobble. The whole 3-DoF rider model produces the same effect of the rider lean as regards weave and the same effect of rider yaw as regards wobble.

The contributions of the present paper to general motorcycle dynamics knowledge can be summarised as follows. A review of the literature on motorcycle dynamics and stability behaviour; this knowledge has been interpreted in order to derive some minimal prerequisites to the motorcycle model, with the aim of conducting a stability analysis. After that, the effect of the tyre response on the wobble damping was analysed, thereby leading to considerations that fuse together with and partially complete the theory exposed by Cossalter [5] and Spierings [6]. Moreover, a possible justification for the well-known weave damping behaviour was given, which was not found in the literature. Finally, the influence of the rider model on stability, which was already studied in previous works, has been summarised, thereby facilitating the interpretation of the effect of the single rider's DoF.

Further development of the present paper could involve the inclusion of a "flexible body" to faithfully reproduce the different frame flexibilities without using lumped stiffnesses.

Author Contributions: F.P. is the leading author who wrote the whole paper. The project and problem formulation were conceptualised by F.P. and D.W.; these authors also built the motorcycle model and produced the results presented in this paper. D.W., A.E., F.D. and A.G. revised the paper critically for important intellectual content. Conceptualisation, F.P. and D.W.; formal analysis, F.P. and D.W.; methodology, F.P. and D.W.; supervision, A.E., D.W., A.G. and F.D.; validation, F.P. and D.W.; visualization, F.P.; writing—original draft, F.P.; writing—review and editing, A.E., D.W., A.G. and F.D. All authors have read and agreed to the published version of the manuscript.

Funding: This research received no external funding.

Acknowledgments: The motorcycle model is completely based on the multibody simulation software "MBSim". The author would like to thank Martin Förg (University of Landshut), who is one of the developers of "MBSim", for the support and suggestions during the building phase of the model. Several structural choices, such as the possibility to select the model DoF, were possible thanks to his contribution.

Conflicts of Interest: The authors declare no conflict of interest.

Nomenclature/Notation

Symbol	Unit	Description
α	rad	Tyre slip angle
α_{ff}	rad	Front fork bending about fork x axis
α_{fr}	rad	Frame torsion at steering head joint
α_{ri}	rad	Rider's upper body lean angle
α_{sw}	rad	Swingarm torsion
β_{ff}	rad	Front fork bending about fork y axis
γ_{ff}	rad	Front fork torsion
γ_{ri}	rad	Rider's upper body yaw rotation
δ	rad	Steer rotation
ΔM_z	N m	Gyroscopic moment due to fork flexibility
Δv_{yC}	m s ⁻¹	Variation of the lateral velocity of the wheel contact point
Δz_{tyre}	m	Tyre carcass compression
θ_{fw}	rad	Front wheel spin angle
θ_{rw}	rad	Rear wheel spin angle
κ	-	Longitudinal slip
ρ	rad	Main frame roll angle
ρ_w	rad	Wheel camber angle
σ	m	Relaxation length
ϕ	rad	Main frame pitch angle
ψ	rad	Main frame yaw angle
${}^B\omega_A$	rad s ⁻¹	Rotational velocity vector of the generic point A in the generic frame B
ω_{fw}	rad s ⁻¹	Front wheel rotational velocity vector
ω_y	rad s ⁻¹	Wheel rotational speed
c_z	N m ⁻¹	Tyre carcass vertical stiffness
d_z	N s m ⁻¹	Tyre carcass vertical damping
${}^{ref}e_i$	-	Unit vector of the <i>i</i> th axis of the "ref" reference frame
F_{yf}	N	Front tyre-lateral force
F_{yr}	N	Rear tyre-lateral force
F_z	N	Tyre vertical load
I_{fw}	kg m ²	Front wheel inertia tensor
I_{rw}	kg m ²	Rear wheel inertia tensor
M_δ	N m	Steer torque
M_{zf}	N m	Front tyre aligning moment
M_{zr}	N m	Rear tyre aligning moment
${}^B\mathbf{S}_A$	-	Transformation matrix from system A to system B
${}^B\mathbf{v}_A$	m s ⁻¹	Absolute velocity vector of the generic point A in the generic frame B
v_{x_C}	m s ⁻¹	Longitudinal speed of the wheel contact point
v_{y_C}	m s ⁻¹	Lateral speed of the wheel contact point
v_{z_C}	m s ⁻¹	Vertical speed of the wheel contact point
y_{ri}	m	Rider's lower body lateral motion
z_f	m	Front suspension travel
z_r	m	Rear suspension travel

Appendix A

Appendix A.1. Geometric Parameters

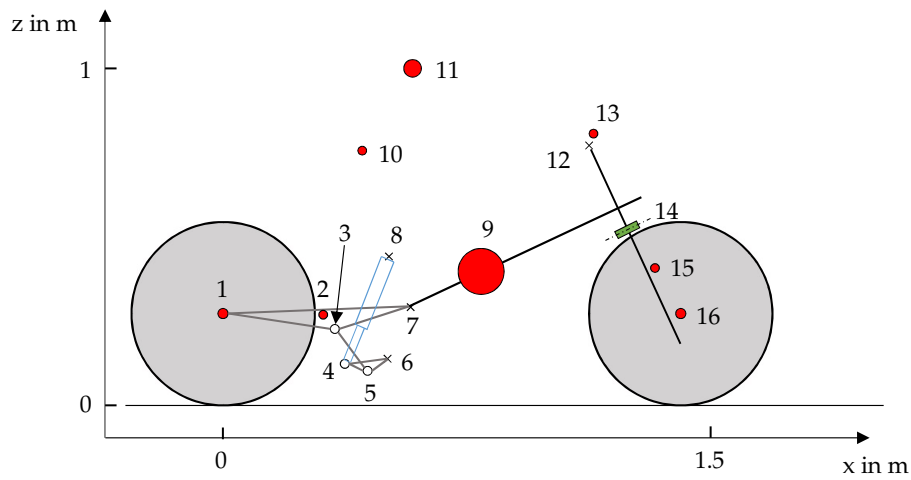


Figure A1. Scheme for the geometric parameters.

Table A1. Dimensions.

Point	x in m	z in m
1	0	0.297
2	0.196	0.3113
3	0.3722	0.2748
4	0.4443	0.1782
5	0.4946	0.1522
6	0.539	0.1878
7	0.549	0.3608
8	0.487	0.4888
9	0.6779	0.4724
10	0.364	0.8438
11	0.415	1.14
12	1.173	0.749
13	1.1803	0.7818
14	1.3036	0.5209
15	1.3125	0.4357
16	1.41	0.282

Table A2. Wheel geometry.

Parameter	Symbol	Value in m
Front wheel radius	r_{fw}	0.282
Front wheel crown radius	$r_{c\,fw}$	0.06
Front wheel rim radius	$r_{rim\,fw}$	0.222
Rear wheel radius	r_{rw}	0.297
Rear wheel crown radius	$r_{c\,rw}$	0.095
Rear wheel rim radius	$r_{rim\,rw}$	0.202

Appendix A.2. Tyre Coefficients

Table A3. Tyre vertical stiffness and damping.

Parameter	Symbol	Value
Front tyre vertical stiffness	$c_{z\text{ fw}}$	130,000 N m ⁻¹
Front tyre vertical damping	$d_{z\text{ fw}}$	800 N s m ⁻¹
Rear tyre vertical stiffness	$c_{z\text{ rw}}$	141,000 N m ⁻¹
Rear tyre vertical damping	$d_{z\text{ rw}}$	800 N s m ⁻¹

The other tyre coefficients used in the present work were taken from [12].

Appendix A.3. Stiffness and Damping

Table A4. Lumped stiffness and damping values. The DoF refer to Figure 1.

DoF	Stiffness	Damping
Frame torsion α_{fr}	163,000 N m rad ⁻¹	100 N m s rad ⁻¹
Front fork bending α_{ff}	55,300 N m rad ⁻¹	20 N m s rad ⁻¹
Front fork bending β_{ff}	55,300 N m rad ⁻¹	20 N m s rad ⁻¹
Front fork torsion γ_{ff}	16,000 N m rad ⁻¹	20 N m s rad ⁻¹
Swingarm torsion α_{sw}	63,700 N m rad ⁻¹	20 N m s rad ⁻¹
Rider rotation about x axis α_{ri}	380 N m rad ⁻¹	34 N m s rad ⁻¹
Rider rotation about z axis γ_{ri}	75.8 N m rad ⁻¹	4.79 N m s rad ⁻¹
Rider arms	1053.4 N m rad ⁻¹	19.28 N m s rad ⁻¹
Rider translation along y axis y_{ri}	38,416 N m rad ⁻¹	981 N s m ⁻¹

Appendix A.4. Suspensions

Table A5. Suspension's parameters.

Parameter	Value
Front spring stiffness	17,000 N m ⁻¹
Front spring unloaded length	0.35 m
Front spring preload	876.231 N
Front compression damping force at 2 m s ⁻¹	203 N
Front rebound damping force at 2 m s ⁻¹	865.8 N
Rear spring stiffness	58,570 N m ⁻¹
Rear spring unloaded length	0.3435 m
Rear spring preload	248.87 N
Rear compression damping force at 1 m s ⁻¹	9600 N
Rear rebound damping force at 1 m s ⁻¹	13,700 N

Appendix A.5. Mass and Inertia

Table A6. Mass parameters.

Parameter	Symbol	Value
Frame mass	m_{fr}	153.716 kg
Rider lower body mass	$m_{ri\ lo}$	11.414 kg
Rider upper body mass	$m_{ri\ ub}$	33.68 kg
Upper fork mass	$m_{ff\ up}$	9.3 kg
Lower fork mass	$m_{ff\ lo}$	6.5 kg
Front wheel mass	m_{fw}	11.9 kg
Swingarm mass	m_{sw}	8 kg
Rear wheel mass	m_{rw}	14.7 kg

Table A7. Inertia parameters.

Parameter	Symbol	Value
Frame inertia	I_{fr}	$\begin{bmatrix} 9.2774 & 0 & 2.267 \\ 0 & 19.0193 & 0 \\ 2.267 & 0 & 13.6702 \end{bmatrix}$ kg m ²
Rider lower body inertia	$I_{ri\ lo}$	$\begin{bmatrix} 0.1163 & 0 & -0.0055 \\ 0 & 0.0942 & 0 \\ -0.0055 & 0 & 0.1036 \end{bmatrix}$ kg m ²
Rider upper body inertia	$I_{ri\ ub}$	$\begin{bmatrix} 1.4280 & 0 & -0.443 \\ 0 & 1.347 & 0 \\ -0.443 & 0 & 0.916 \end{bmatrix}$ kg m ²
Upper fork inertia (z axis \equiv steer axis)	$I_{ff\ up}$	$\begin{bmatrix} 0.5 & 0 & 0 \\ 0 & 0.4 & 0 \\ 0 & 0 & 0.13 \end{bmatrix}$ kg m ²
Lower fork inertia (z axis \equiv steer axis)	$I_{ff\ lo}$	$\begin{bmatrix} 0.3 & 0 & 0 \\ 0 & 0.25 & 0 \\ 0 & 0 & 0.09 \end{bmatrix}$ kg m ²
Front wheel inertia	I_{fw}	$\begin{bmatrix} 0.27 & 0 & 0 \\ 0 & 0.484 & 0 \\ 0 & 0 & 0.27 \end{bmatrix}$ kg m ²
Swingarm inertia	I_{sw}	$\begin{bmatrix} 0.02 & 0 & 0 \\ 0 & 0.259 & 0 \\ 0 & 0 & 0.259 \end{bmatrix}$ kg m ²
Rear wheel inertia	I_{rw}	$\begin{bmatrix} 0.383 & 0 & 0 \\ 0 & 0.638 & 0 \\ 0 & 0 & 0.383 \end{bmatrix}$ kg m ²

References

1. Sharp, R.S. Stability, Control and Steering Responses of Motorcycles. *Veh. Syst. Dyn.* **2001**, *35*, 291–318. [CrossRef]
2. Cossalter, V. *Motorcycle Dynamics*, 2nd ed.; Lulu Press: Morrisville, NC, USA, 2006.
3. Sharp, R.S. The stability and control of motorcycles. *J. Mech. Eng. Sci.* **1971**, *13*, 316–329. [CrossRef]
4. Koch, H. *Zusammenhänge und Einflüsse von Lebensalter, Fahrerfahrung und Motorleistung auf die Unfallverwicklung von Motorradfahranfängern*; VDI-Berichte: Düsseldorf, Germany, 1987.
5. Cossalter, V.; Lot, R.; Massaro, M. The influence of frame compliance and rider mobility on the scooter stability. *Veh. Syst. Dyn.* **2007**, *45*, 313–326. [CrossRef]
6. Splerings, P.T.J. The Effects of Lateral Front Fork Flexibility on the Vibrational Modes of Straight-Running Single-Track Vehicles. *Veh. Syst. Dyn.* **1981**, *10*, 21–35. [CrossRef]
7. Cossalter, V.; Lot, R.; Massaro, M. An advanced multibody code for handling and stability analysis of motorcycles. *Meccanica* **2011**, *46*, 943–958. [CrossRef]

8. Koenen, C.; Pacejka, H.B. The Influence of Frame Elasticity and Simple Rider Body Dynamics on Free Vibrations of Motorcycles in Curves. *Veh. Syst. Dyn.* **1981**, *10*, 70–73. [[CrossRef](#)]
9. Cossalter, V.; Doria, A.; Mitolo, L. *Inertial and Modal Properties of Racing Motorcycles*; SAE Technical Papers; SAE International: Warrendale, PA, USA, 2002.
10. Wisselmann, D. *Motorrad-Fahrdynamik-Simulation. Modellbildung, Validierung und Anwendung*. Ph.D. Thesis, VDI-Berichte, Dachau, Germany, 1992.
11. Schindler, T.; Förg, M.; Friedrich, M.; Schneider, M.; Esefeld, B.; Huber, R.; Zandler, R.; Ulbrich, H. Analysing Dynamical Phenomenons: Introduction to MBSim. In Proceedings of the 1st Joint International Conference on Multibody System Dynamics, Lappeenranta, Finland, 25–27 May 2010.
12. Sharp, R.S.; Evangelou, S.A.; Limebeer, D.J.N. Advances in the Modelling of Motorcycle Dynamics. *Multibody Syst. Dyn.* **2004**, *12*, 251–283. [[CrossRef](#)]
13. Limebeer, D.J.N.; Massaro, M. *Dynamics and Optimal Control of Road Vehicles*; Oxford University Press: Oxford, UK, 2018.
14. Cossalter, V.; Doria, A.; Massaro, M.; Taraborrelli, L. Experimental and numerical investigation on the motorcycle front frame flexibility and its effect on stability. *Mech. Syst. Signal Process.* **2015**, *60–61*, 452–471. [[CrossRef](#)]
15. Meirovitch, L. *Elements of Vibration Analysis*; Mc Grow Hill: New York, NY, USA, 1975.
16. Doria, A.; Favaron, V.; Taraborrelli, L.; Roa, S. Parametric analysis of the stability of a bicycle taking into account geometrical, mass and compliance properties. *Int. J. Veh. Des.* **2017**, *75*, 91–123. [[CrossRef](#)]
17. Doria, A.; Roa, S. On the influence of tyre and structural properties on the stability of bicycles. *Veh. Syst. Dyn.* **2018**, *56*, 947–966. [[CrossRef](#)]
18. Klinger, F.; Nusime, J.; Edelmann, J.; Plöchl, M. Wobble of a racing bicycle with a rider hands on and hands off the handlebar. *Veh. Syst. Dyn.* **2014**, *52*, 51–68. [[CrossRef](#)]
19. Sharp, R.S.; Alstead, C.J. The Influence of Structural Flexibilities on the Straight-running Stability of Motorcycles. *Veh. Syst. Dyn.* **1980**, *9*, 327–357. [[CrossRef](#)]
20. Plöchl, M.; Edelmann, J.; Angrosch, B.; Ott, C. On the wobble mode of a bicycle. *Veh. Syst. Dyn.* **2012**, *50*, 415–429. [[CrossRef](#)]
21. Roa, S.; Doria, A.; Muñoz, L. Optimization of the Bicycle Weave and Wobble Modes. *Am. Soc. Mech. Eng.* **2018**, *3*. [[CrossRef](#)]
22. Diermeyer, F.; Eisele, A. Lecture notes of the course Motorradtechnik. 2018, Unpublished manuscript.
23. Taraborrelli, L.; Favaron, V.; Doria, A. The effect of swingarm stiffness on motorcycle stability: experimental measurements and numerical simulations. *Int. J. Veh. Syst. Model. Test.* **2017**, *12*, 240. [[CrossRef](#)]
24. Weir, D.H.; Zeller, J.W. Experimental investigation of the transient behaviour of motorcycles. *SAE Trans.* **1979**, *88*, 962–978.
25. De Vries, E.; Pacejka, H.B. Motorcycle Tyre Measurements and Models. *Veh. Syst. Dyn.* **1998**, *29*, 280–298. [[CrossRef](#)]
26. Pacejka, H.B.; Besselink, I. *Tire and Vehicle Dynamics*, 3rd ed.; Butterworth-Heinemann: Oxford, UK, 2012.
27. Evangelou, S.A.; Limebeer, D.J.N.; Sharp, R.S.; Smith, M.C. Mechanical steering compensators for high-performance motorcycles. *J. Appl. Mech. Trans.* **2007**, *74*, 332–346. [[CrossRef](#)]
28. Sharp, R.S.; Limebeer, D.J.N. A Motorcycle Model for Stability and Control Analysis. *Multibody Syst. Dyn.* **2001**, *6*, 123–142. [[CrossRef](#)]
29. Cossalter, V.; Lot, R.; Maggio, F. A Multibody Code for Motorcycle Handling and Stability Analysis with Validation and Examples of Application. In *SAE International400 Commonwealth Drive*; SAE Technical Paper Series; SAE International: Warrendale, PA, USA, 2003. [[CrossRef](#)]
30. Limebeer, D.J.N.; Sharma, A. Burst Oscillations in the Accelerating Bicycle. *J. Appl. Mech. Trans.* **2010**, *77*, 061012. [[CrossRef](#)]
31. Roe, G.E.; Thorpe, T.E. A solution of the low-speed wheel flutter instability in motorcycles. *J. Mech. Eng. Sci.* **1976**, *18*, 57–65. [[CrossRef](#)]
32. Cossalter, V.; Lot, R.; Maggio, F. The Modal Analysis of a Motorcycle in Straight Running and on a Curve. *Meccanica* **2004**, *39*, 1–16. [[CrossRef](#)]
33. Limebeer, D.J.N.; Sharp, R.S.; Evangelou, S.A. Motorcycle Steering Oscillations due to Road Profiling. *J. Appl. Mech. Trans.* **2002**, *69*, 724–739. [[CrossRef](#)]

34. Sharp, R.S. The Influence of the Suspension System on Motorcycle Weave-mode Oscillations. *Veh. Syst. Dyn.* **1976**, *5*, 147–154. [[CrossRef](#)]
35. Lot, R. A Motorcycle Tire Model for Dynamic Simulations: Theoretical and Experimental Aspects. *Meccanica* **2004**, *39*, 207–220. [[CrossRef](#)]
36. Evangelou, S.A.; Limebeer, D.J.N.; Tomas-Rodriguez, M. Suppression of Burst Oscillation in Racing Motorcycle. *J. Appl. Mech.* **2013**, *80*, 011003. [[CrossRef](#)]
37. Karnopp, D. *Vehicle Dynamics, Stability, and Control*, 2nd ed.; CRC Press Taylor and Francis: Boca Raton, FL, USA, 2013.
38. Robbins, D.H. *Anthropometry of Motor Vehicle Occupants: Final Report October 1980–December 1983*; University of Michigan Transportation Research Inst: Ann Arbor, MI, USA, 1983; Volume 83-53-2.
39. Wunram, K.; Eckstein, L.; Rettweiler, P. *Potenzial Aktiver Fahrwerke zur Erhöhung der Fahrsicherheit von Motorrädern: Bericht zum Forschungsprojekt FE 82.328/2007*; Berichte der Bundesanstalt für Strassenwesen, Fahrzeugtechnik; Wirtschaftsverl. NW Verl. für Neue Wiss: Bremerhaven, Germany, 2011; Volume 81.
40. Sharp, R.S.; Limebeer, D.J.N. On steering wobble oscillations of motorcycles. *Proc. Inst. Mech. Eng. Part C J. Mech. Eng. Sci.* **2004**, *218*, 1449–1456. [[CrossRef](#)]
41. Doria, A.; Formentini, M.; Tognazzo, M. Experimental and numerical analysis of rider motion in weave conditions. *Veh. Syst. Dyn.* **2012**, *50*, 1247–1260. [[CrossRef](#)]
42. Cossalter, V.; Doria, A.; Lot, R.; Massaro, M. The effect of rider's passive steering impedance on motorcycle stability: Identification and analysis. *Meccanica* **2011**, *46*, 279–292. [[CrossRef](#)]
43. Sequenzia, G.; Oliveri, S.M.; Fatuzzo, G.; Calì, M. An advanced multibody model for evaluating rider's influence on motorcycle dynamics. *Proc. Inst. Mech. Eng. Part K J. Multi-Body Dyn.* **2015**, *229*, 193–207. [[CrossRef](#)]
44. Mitschke, M. *Dynamik der Kraftfahrzeuge*; Springer: Berlin/Heidelberg, Germany, 1972.
45. Schröter, K.G. Brake Steer Torque Optimized Corner Braking of Motorcycles. Ph.D. Thesis, Technische Universität Darmstadt, Darmstadt, Germany, 2015.



© 2020 by the authors. Licensee MDPI, Basel, Switzerland. This article is an open access article distributed under the terms and conditions of the Creative Commons Attribution (CC BY) license (<http://creativecommons.org/licenses/by/4.0/>).